SUPPLEMENTARY MATERIAL

Southern Laurentide ice-sheet retreat synchronous with rising boreal summer insolation

David J. Ullman*, Anders E. Carlson, Allegra N. LeGrande, Angus K. Moore, Faron S. Anslow, Marc Caffee, Kent M. Syverson, Joseph M. Licciardi
*Corresponding author: dullman@coas.oregonstate.edu

Field methods and site descriptions

- We limit the impact of landscape change (Schulte et al., 2007) and post-glacial disturbance on exposure surfaces through the sampling the surfaces of large quartz-bearing glacial erratics in regions of WI with minimal human disturbance. Large, far-travelled glacial erratics have been shown to exhibit less cosmogenic inheritance than bedrock surfaces, particularly in regions where cold-based ice may have limited subglacial scouring (Corbett et al., 2013). We focus our site selection on stable topographic highs away from collapsed ice features with minimal till cover. Due to such geomorphic setting, topographic shielding correction was unnecessary for all of the samples. We preferentially selected boulders that were large in size (>1 m in diameter and height) and showed minimal signs of surface erosion (no pitting or spalling). For individual sample information on location, elevation, and thickness see Table DR1.
- The Baraboo Hills are a Proterozoic quartzite syncline in south-central WI. The eastern half of this range was covered by the sLIS during the LGM, depositing erratic boulders on top of the quartzite bedrock as part of the Johnstown LGM moraine (Clayton and Attig, 1990). We sampled far-traveled granite boulders in addition to local quartzite and sandstone boulders deposited in a prominent boulder-train moraine resting directly on bedrock (site sGBL) (Fig. DR1).
- About 10 km to the northeast, the i-sGBL site lies atop another quartzite hill, which was covered by ice during the LGM and exposed following ice-retreat from the terminal moraine (Fig. DR1) (Clayton and Attig, 1990). The lack of moraines in between i-sGBL and sGBL indicates a continuous retreat pattern between the two sampling locations.
- The Blue Hills are an outcrop of erosion-resistant quartzite in north-central WI of similar age to the Baraboo Hills (Mudrey et al., 1982). LGM ice covered most of the bedrock topographic highs in the Blue Hills. Site CL is along this maximum extent of the LGM phase of the Chippewa Lobe (Attig et al., 1985; Johnson, 1986), whereas the i-CL site is located ~12 km to the northeast of the terminal moraine (Fig. DR2). No moraines exist between CL and i-CL suggesting no stable ice margin positions between these two sites.
- The Gogebic Mountains (site GM) in northern Wisconsin are a high-relief set of parallel ridgelines of metasedimentary and meta-volcanic bedrock (Cannon et al., 2007). We sampled glacial erratics at GM resting directly on bedrock of these flat-topped topographic highs (Fig. DR3, DR4).
- The northern Green Bay Lobe (nGBL) samples come from a high-relief section of the prominent LGM Hancock Moraine that is correlative to the Johnstown Moraine (Fig. DR5) (Attig et al., 1985). The samples are from 2 stable sections of the Hancock Moraine crest, away from ice-collapse features (Fig. DR6, DR7).
- The inner nGBL site (i-nGBL) lies ~15 km east of the LGM extent of the LIS in the interlobate region of the Langlade and Green Bay Lobes, where the recessional Summit Lake Moraine of the Langlade Lobe and Bowler Moraine of the Green Bay Lobe connect (Attig et al., 1985; Fig. DR4, DR8). The Summit Lake Moraine is correlative with Tiger Cat and Flambeau moraines to the west. The Bowler Moraine continues south where it is called the Green Lake Moraine in southeast WI. We sampled boulders from a

constructional deposit that accumulated in an ice cavity (Mickelson, 1986). The exposure ages from these boulders are associated with the retreat of ice from this location.

Laboratory methods

- Sample preparation and isolation of BeO was conducted in the Cosmogenic Isotope Laboratory at the University of Wisconsin-Madison (UW).
- Each sample was crushed and sieved to separate the 425-841 μm grain-size fraction. The quartz fraction was separated using a Frantz Magnetic Separator to remove mafic grains, followed by etchings with HCl and dilute HF/HNO_3.
- The purity of this quartz fraction was verified through elemental analysis by Inductive-Coupled Plasma Atomic Emission Spectrometry at University of Colorado-Boulder.
- After addition of Be carrier, the BeO was isolated through a series of dissolution, oxidation, anion/cation removal, pH adjustments, and final sample drydown.
- $^{10}Be/^{9}Be$ ratios were measured by accelerator mass spectrometry (AMS) at Purdue Rare Isotope Measurement (PRIME) Laboratory at Purdue University.
- Throughout this project, the UW Cosmogenic Lab made improvements in the ^{9}Be purity of its standard. Initial use of a commercially available Be standard resulted in blank AMS-measured $^{10}Be/^{9}Be$ ratios that averaged to be $12.2 \times 10^{-15} \pm 0.9 \times 10^{-15}$ (Claritas, Table DR1, ratio expressed as long-term laboratory mean with standard error as uncertainty). An intermediate standard of higher purity resulted in $^{10}Be/^{9}Be$ ratios that averaged to be $3.4 \times 10^{-15} \pm 0.4 \times 10^{-15}$ (Merck, Table DR1). Use of a new ultra-pure standard developed at Oregon State University (Murray et al., 2012) used in later analysis resulted in average procedural blank $^{10}Be/^{9}Be$ ratios of $2.0 \times 10^{-15} \pm 0.3 \times 10^{-15}$ (OSU Blue, Table DR1).
- Sample ^{10}Be concentrations are shown in Table DR1.

Exposure age calculation

- We used the online CRONUS-Earth calculator (http://hess.ess.washington.edu/) to determine exposure ages (Balco et al., 2008) using the northeast North American production rate (NENA, Balco et al., 2009).
- All relevant sample data entered into the online CRONUS-Earth surface exposure calculator is presented in Table DR1.
- Our analysis throughout the text uses the Lal-Stone time-dependent scaling scheme (Lal, 1991; Stone, 2000) for calculating both the new chronology of this study as well as in recalculating the existing ^{10}Be dates (Colgan et al., 2002; Balco et al., 2009).
- Use of any of the other scaling schemes (Stone, 2000; Desilets et al., 2006; Dunai, 2001; Lifton et al., 2005) does not change the interpretation (within the uncertainty of measurement).

Removal of outliers

- For the timing of initial retreat from the terminal moraines in Wisconsin (sites sGBL, nGBL, and CL), we exclude all ages that are older than 30 ka and younger than 17.5 ka for the Green Bay Lobe dates, because ^{14}C dates indicate that the sLIS was not present in Wisconsin until after 30 ka (Black, 1976; Attig et al., 1985; Dyke et al., 2002; Clark et al., 2009) and must have retreated from the Green Bay Lobe terminal moraines before 17.5 ka, based on the oldest calibrated minimum-limiting ^{14}C age from Valders Quarry of 17.7±0.2 ka (Maher et al., 1998) (Fig. DR9).
- After this *a-priori* removal of outliers and because our data sets are normally distributed

based on the Shapiro-Wilks test, we use Chauvenet's statistical test to exclude ages that have a large deviation from the sample set mean compared with the standard deviation and accounting for the number of samples (Clark et al., 2009; Rinterknecht et al., 2006).

- We have identified 13 outliers that were removed before calculating site averages and standard errors. Eleven outliers were excluded by *a-priori* removal; two outliers were excluded based on Chauvenet's criterion.
- Outliers that are removed are shown in Fig. DR9.
- Because the scatter in ages for a given sample site is larger than the analytical uncertainty of each individual measurement, we calculate the straight mean and standard error of the mean as the best estimate of the true age of deglaciation and its geological uncertainty for sites CL, nGBL, sGBL, i-nGBL, and GM (Bevington and Robinson, 2002).
- For sites i-CL and i-sGBL, where we only have two samples per site, the difference between ages is equal to or smaller than the analytical uncertainty of each measurement. Therefore we present the error-weighted mean and uncertainty for these sites, as the standard error between the consistent ages does not provide an adequate representation of overall uncertainty (Bevington and Robinson, 2002).

Construction of time-distance diagrams

- In Fig. 2 of the text, we construct time-distance diagrams for the Green Bay, Lake Michigan, and Miami-Scioto Lobes using the bracketing ^{14}C ages on ice-margin advances and retreats. These diagrams have been previously published (see below).
- All radiocarbon ages discussed are calibrated using Calib 7.0 and IntCal13 (Stuiver and Reimer, 1993; Reimer et al., 2013).
- All information necessary to construct these diagrams is provided in Table DR2 and the respective publications.
- The Miami-Scioto Lobe time-distance curve (Fig. 2f) is an updated version of Eckberg et al. (1993), based on ages from Lowell et al. (1990), Dyke (2004) and Glover et al. (2011).
- The Lake Michigan Lobe time-distance curve (Fig. 2g) is an updated version of the Hansel and Johnson (1992) record from Curry and Petras (2011).
- The Green Bay Lobe time-distance curve (Fig. 2h) is from a combination of dates, and was recently summarized in Hooyer et al. (2007) (see Table DR2 for list of ages).
- In Fig. 2i, we draw a similar record of retreat for the northern Green Bay Lobe, constrained by the correlation of the ice margin positions (following Hooyer et al., 2007).
- Since chronological information for the Chippewa Lobe is limited prior to this study, we draw the time-distance diagram of Fig. 2j solely using our new ^{10}Be chronology.

Surface mass balance modeling

- To simulate the surface mass balance (SMB) of the southern LIS, we conducted paired simulations of a fully-coupled atmosphere-ocean general circulation model (GCM) (NASA GISS ModelE2-R; Schmidt et al., 2014) and a surface energy balance model (SEBM) (Anslow et al., 2008; Carlson et al., 2009).
- The paired GCM-SMB approach used here forces the SMB calculations with an equilibrium climate from the GCM, given a particular set of ice sheet and solar/greenhouse gas forcings.
- The current version of ModelE2-R has an atmosphere resolution of 2 degrees latitude by 2.5 degrees longitude with 40 vertical layers up to 0.1 mb and an ocean resolution of 1 degree latitude by 1.25 degrees longitude with 32 depth layers.
- We conducted three separate simulations at 24 ka, 21 ka, and 19 ka using the appropriate

insolation of each time period due to changes in orbital parameters (Berger and Loutre, 1991) (see Ullman et al., 2014). We also ran a simulation at 16.5 ka that included appropriate insolation forcing and atmospheric greenhouse gas concentrations.

- We employed the LGM global ice-sheet topography of ICE-5G (Peltier, 2004) but substituted an alternative reconstruction of the LIS over North America (Licciardi et al., 1998). At the LGM, the Laurentide Ice Sheet abutted the Cordilleran Ice Sheet to the west, and the interface between the Licciardi et al. (1998) reconstruction of the LIS and the ICE-5G reconstruction of the Cordilleran Ice Sheet leads to a discontinuity in ice elevation, as the Licciardi et al. (1998) reconstruction does not include ice-buttressing effects of the adjacent Cordilleran Ice Sheet. However, we focus our calculations of surface mass balance to the southern margin alone, away from this interface between ice sheet masses.
- The Licciardi et al. (1998) reconstruction is based on a flow-line model that simulates ice-sheet dynamics over deformable and rigid beds. The advantage of this reconstruction for this study is its ability to resolve the low elevation margins of the sLIS that agrees with observations of inferred topographic gradients along the southern margin (Clark, 1992). Due to these geologic constraints, the Licciardi et al. reconstruction may capture of the topographic gradient and resolution of the equilibrium line altitude close to the ice margin better than other reconstructions (e.g., Fig. DR10) (Peltier, 2004; Clark et al., 1996; Licciardi et al., 1998; Tarasov and Peltier, 2004; Argus and Peltier, 2010; Lambeck et al., 2010; Tarasov et al., 2012).
- The Licciardi et al. (1998) model does not include the divergence of ice along flowlines with transverse spread. This limitation may result in greater ice elevations relative to regions with radial spreading centers, but such spreading centers are well above the equilibrium line altitude of the model and the inferred elevation bias may have little effect on surface mass balance for the sLIS.
- Each time slice SMB simulation was forced by temporally interpolated, daily climatologies of relevant parameters (surface air temperature, precipitation, wind speed, relative humidity, and surface radiation fluxes), which were calculated using the final 100 years of equilibrium GCM output.
- For the downscaling of relatively coarse-resolution GCM output (2 x 2.5 degree) to the higher-resolution (50 km) ice sheet topography of Licciardi et al. (1998), we use a temperature lapse rate of 5 °C km^{-1} and a precipitation lapse scaling of 0.1 km^{-1}, following Carlson et al. (2009; 2012), and suggested by previous climate reconstructions above ice sheets (Pollard et al., 2000; Marshall et al., 2002; Abe-Ouchi et al., 2007). Since we fix these lapse rates across each of the time slice simulations, varying them within the range of other lapse estimates does not significantly impact our resulting mass balance anomalies from the 24 ka results.
- We performed sensitivity tests and found that since the elevation distance is typically small between the GCM and SMB model grids; varying the parameters has a minimal effect on absolute surface mass balance that is well within the range of balances that arise from the changes in surface roughness and albedo decay. Testing at differing resolutions at and below 50 km x 50 km did not impact the model surface mass balance anomalies (Carlson et al., 2009).
- We use snow/ice roughness and albedo decay rate parameters that match average modern observations from the Greenland and Antarctic Ice Sheets (Carlson et al., 2009; Grainger and Lister, 1966; Duynkerke and van den Broeke, 1994; Greuell and Konzelmann, 1994; Smeets and van den Broeke, 2008).
- Because we are interested in the effects that changes in radiative forcing from Earth's orbit and greenhouse gases have on the southern LIS SMB, we only look at the change in SMB relative to the 24 ka simulation (Fig. DR10).

- The 16.5 ka simulation are the results of a hybrid SMB simulation, which uses a 16.5 ka GCM climate forcing downscaled and applied to the LGM (21 ka) ice-sheet topography. In the GCM resolution, the differences between 21 and 16.5 ka ice sheets are small (both in extent and ice sheet elevation), so the downscaling to the higher resolution ice sheet topography is similar to the straight LGM (24-19 ka) downscaling.
- Total surface mass balance across the southern LIS is negative and decreasing with increasing insolation forcing: -330 Gt yr-1 (24 ka), -540 Gt yr^{-1} (21 ka), -690 Gt yr^{-1} (19 ka). The 16.5 ka forcing with increases in both insolation and greenhouse gas forcing results in a southern LIS surface mass balance of -1320 Gt yr^{-1} (Fig. DR12). We focus the results as anomalies in the main text so as to minimize uncertainty that may be inherent to our model design.

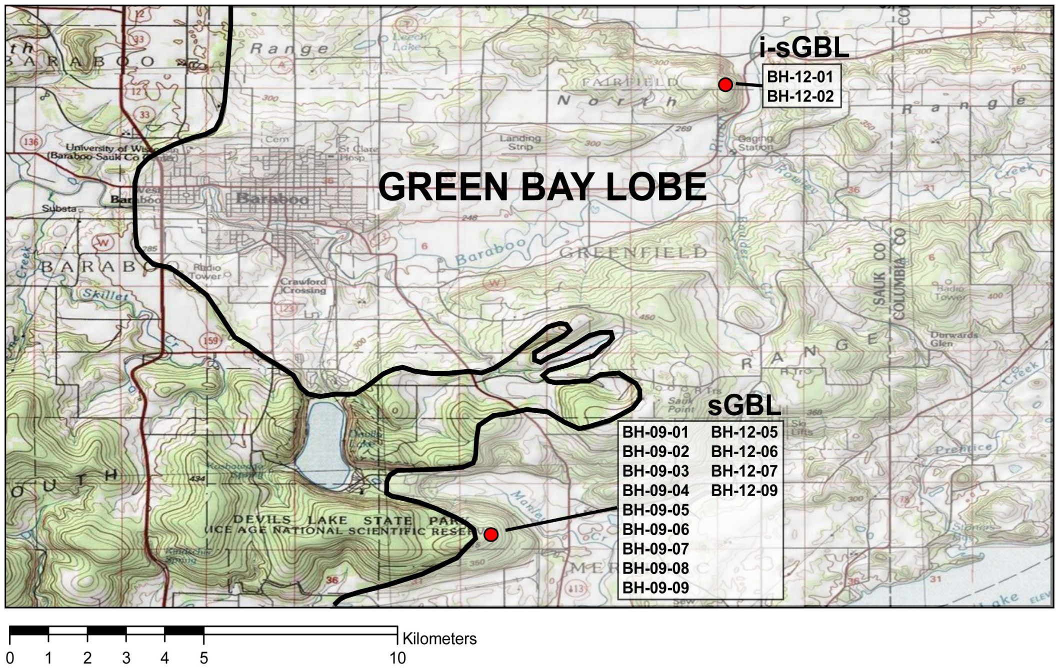

Fig. DR1. Topographic map of the sGBL and i-sGBL sampling locations and the samples collected at each site (shown as red circles). Extent of LGM ice is shaded in white, with a rough outline of the terminal moraine drawn with the heavy black line. Underlying topographic map provided by the USGS and the National Geographic Society (© 2011).

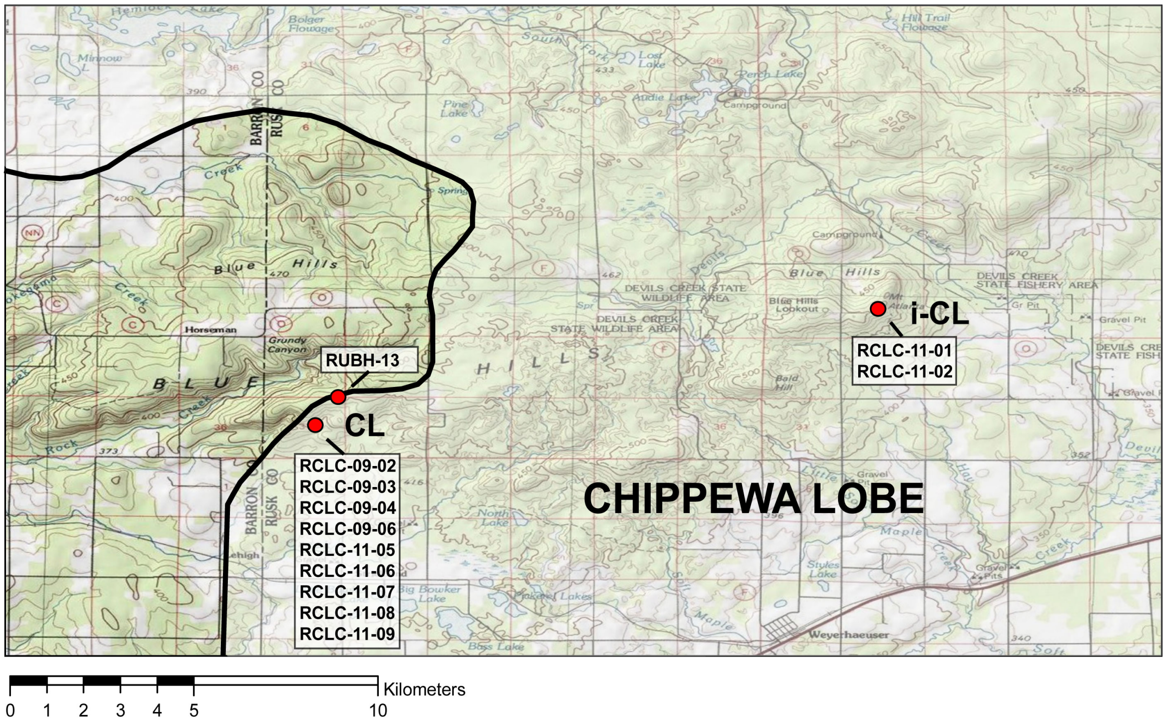

Fig. DR2. Topographic map of the CL and i-CL sampling locations and the samples collected at each site (shown as red circles). Extent of LGM extent of the Chippewa Lobe is shaded in white, with a rough outline of the terminal moraine drawn with the heavy black line. Underlying topographic map provided by the USGS and the National Geographic Society (© 2011).

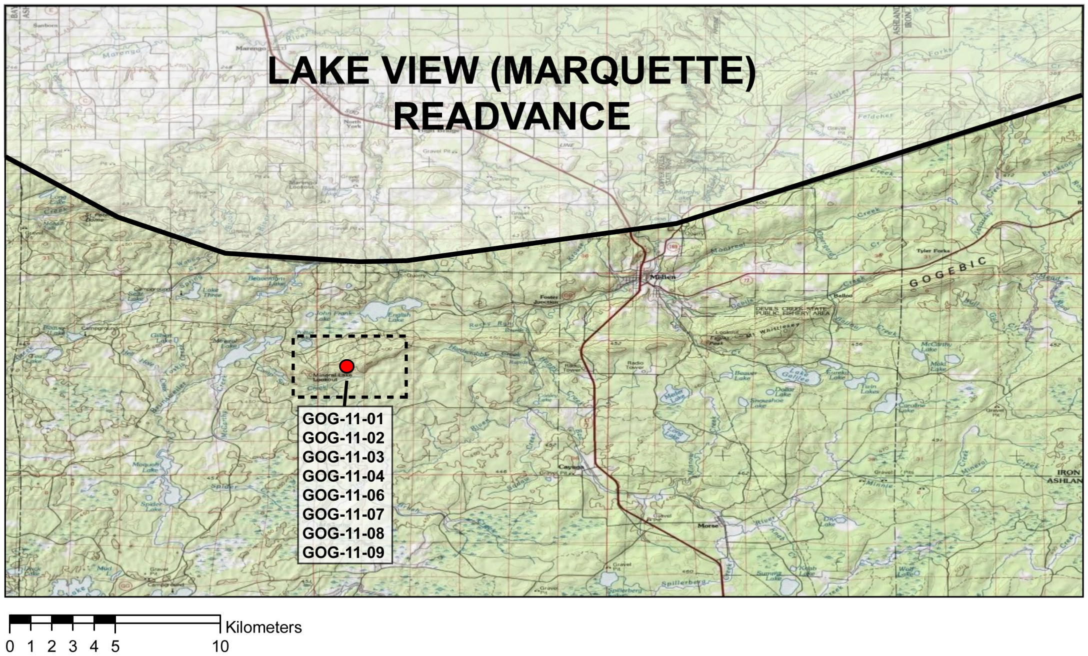

Fig. DR3. Regional topographic map of the GM sampling location and the samples collected at the site (shown as red circle). The parallel ridgelines of the Gogebic Range can be seen in eastern portion of the map. The sampling location is on one of the westernmost bedrock arms of this range. The rough extent of the Lake View Phase ice margin is shaded in white. This readvance occurred during Younger Dryas cold interval and is correlative with the Marquette Phase to the east (Lowell et al., 1999a). There is no evidence to suggest that this readvance overtopped the Gogebic Range. Region displayed in Fig. DR4 denoted by the black dashed box. Underlying topographic map provided by the USGS and the National Geographic Society (© 2011).

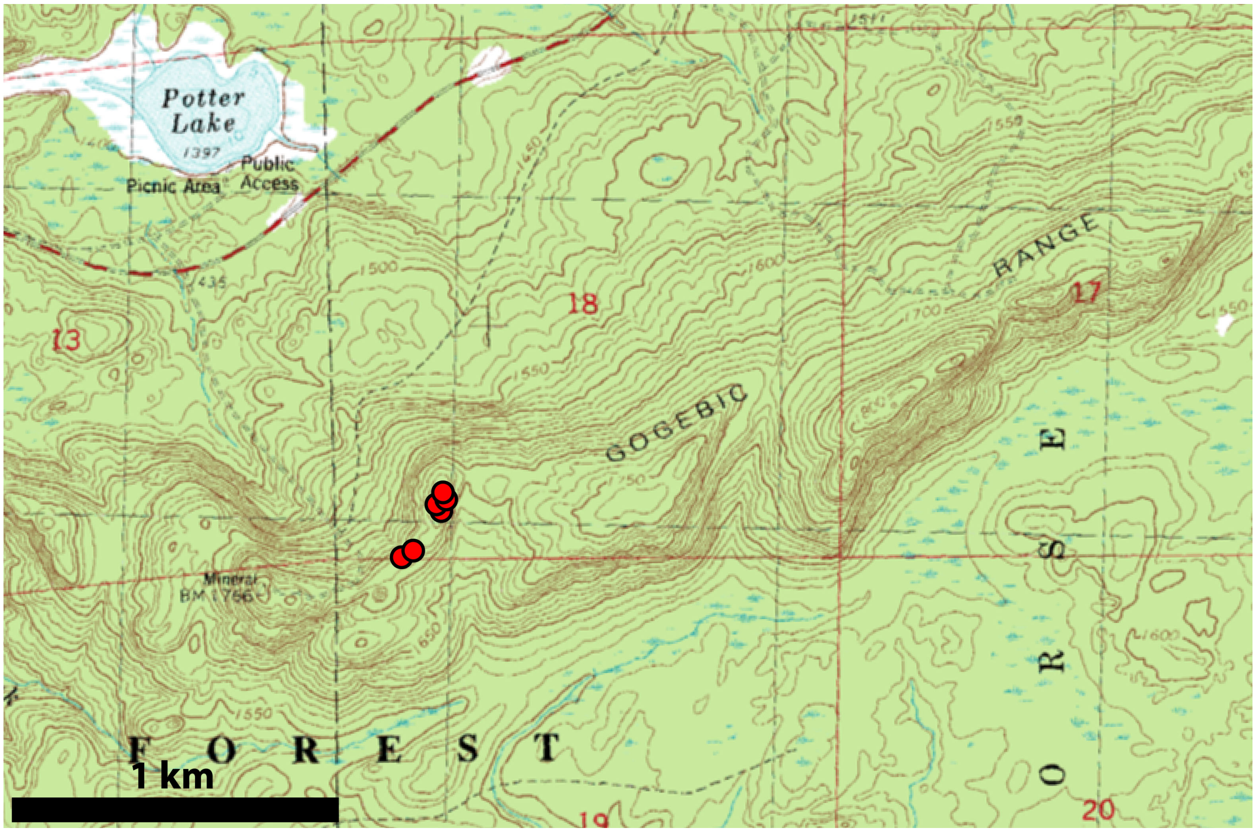

Fig. DR4. Map of topography immediately surrounding GM sampling sites (red circles). Underlying topographic map (1:24,000 scale, 10 foot contour interval) provided by the USGS and the National Geographic Society (© 2011).

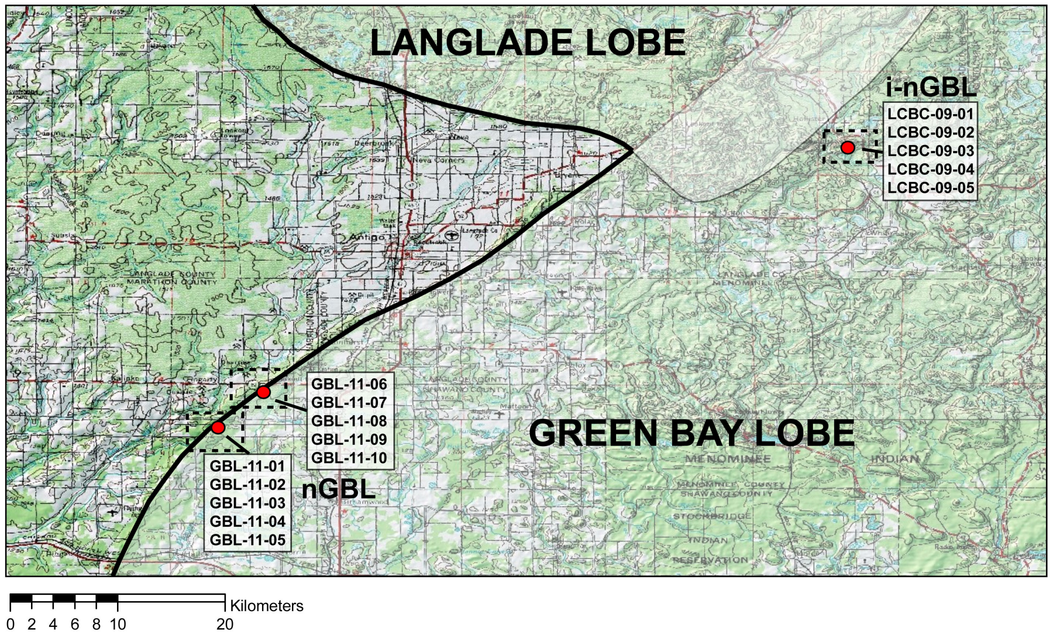

Fig. DR5. Regional topographic map of the nGBL and i-nGBL (LCBC) sampling locations and the samples collected at each site (shown as red circles). This map shows the confluence of the Langlade and Green Bay Lobes shaded in white, with their outer LGM extents drawn with the heavy black line. Regions displayed in Fig. DR6-DR8 denoted by the black dashed boxes. Underlying topographic map provided by the USGS and the National Geographic Society (© 2011).

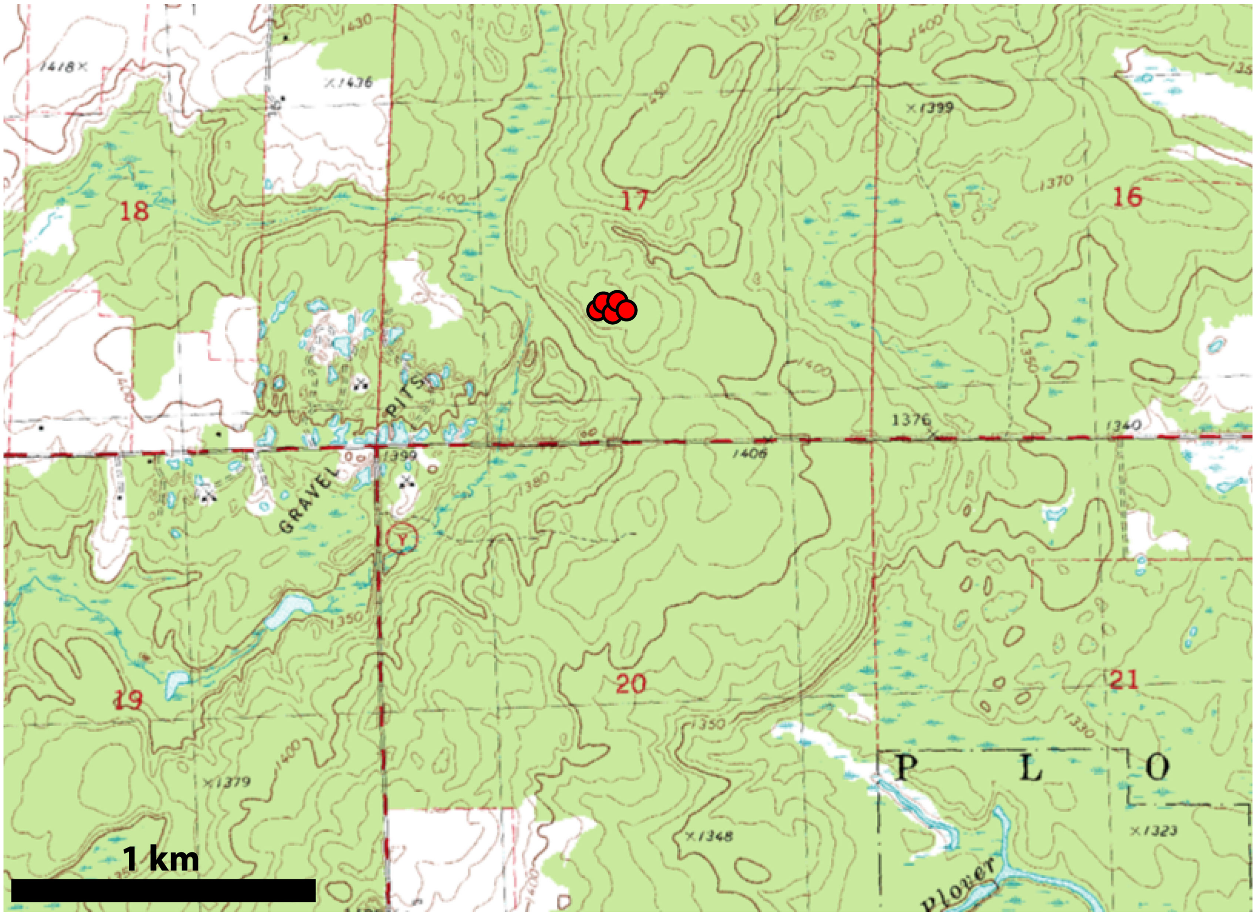

Fig. DR6. Map of topography immediately surrounding sampling sites GBL-11-01 through GBL-11-05 (red circles). Ice-collapse features are evidence along this moraine, but the sampling sites come from a stable and flat topographic high away from hummocky terrain. Underlying topographic map (1:24,000 scale, 10 foot contour interval) provided by the USGS and the National Geographic Society (© 2011).

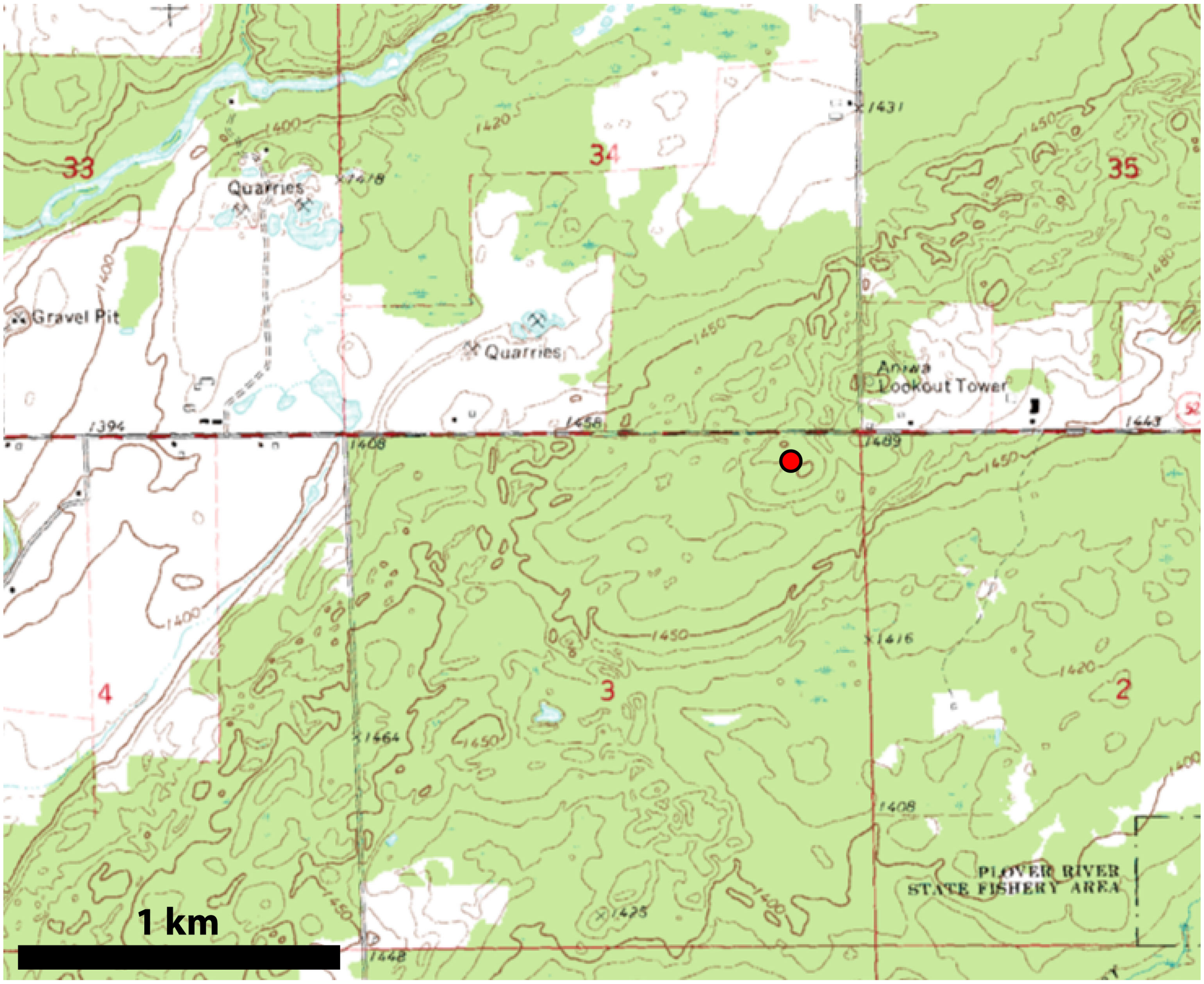

Fig. DR7. Map of topography immediately surrounding sampling sites GBL-11-06 through GBL-11-10 (red circle). The prominent terminal moraine of this site can be seen running from the southwest to northeast corners of this map, with the flatter outwash plain evident in the northwest corner. The sampling sites come from a stable and flat topographic high away from some of the collapsed features on this moraine. Underlying topographic map (1:24,000 scale, 10 foot contour interval) provided by the USGS and the National Geographic Society (© 2011).

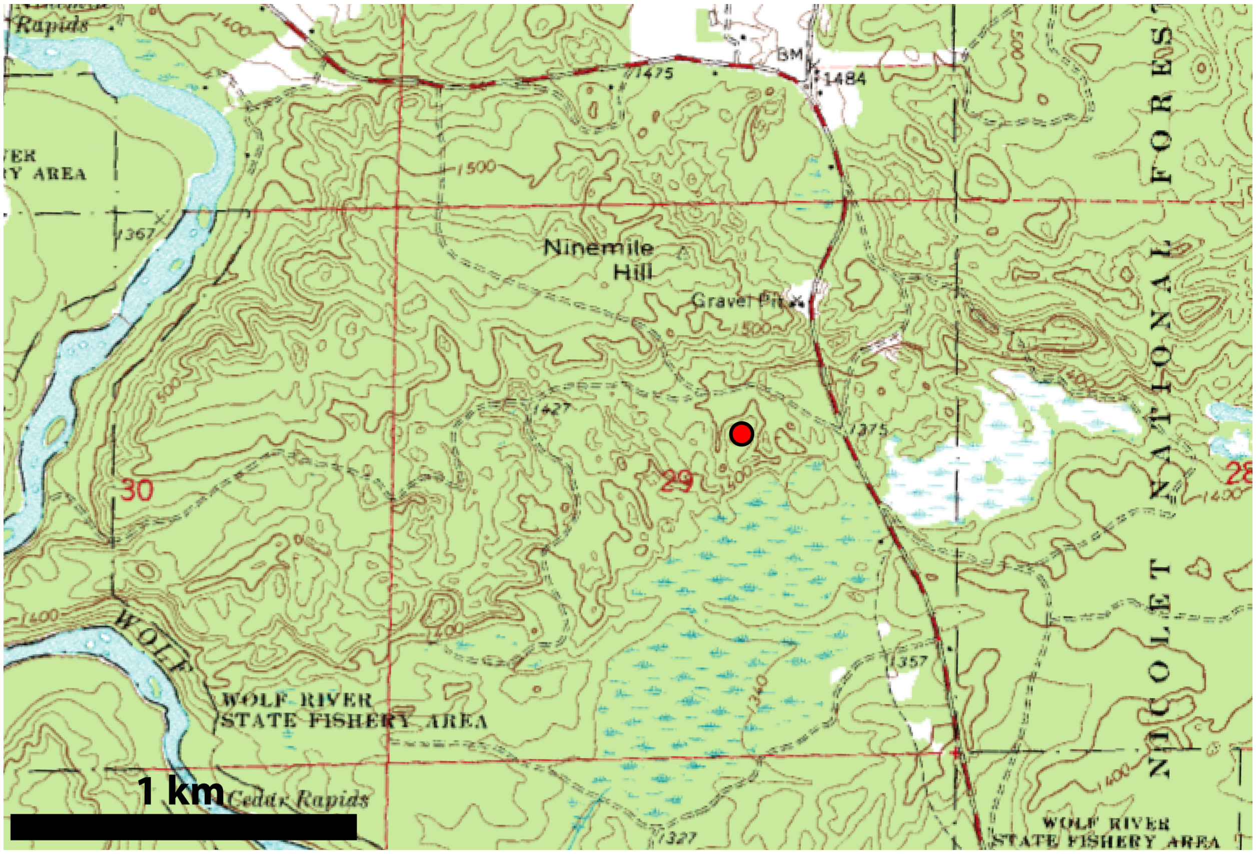

Fig. DR8. Map of topography immediately surrounding i-nGBL sampling sites (red circle). Underlying topographic map (1:24,000 scale, 10 foot contour interval) provided by the USGS and the National Geographic Society (© 2011).

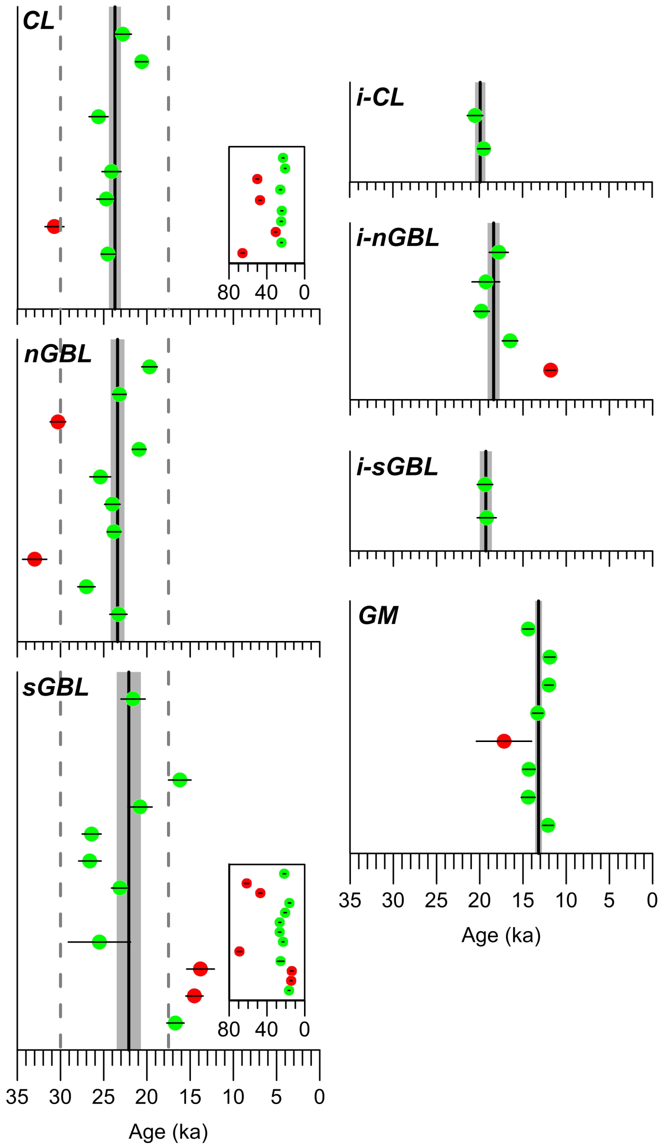

Fig. DR9. Individual ^{10}Be exposure ages for each of the sampling sites (denoted in upper left corner of each plot). Green symbols indicate ages used in site age calculation, and red symbols indicate outliers not included in the site age. Error bars for each age are 1σ analytical uncertainty. Vertical black lines show mean age for each site with shaded gray bars indicating the 1σ uncertainty range (standard error of the mean or error-weighted sigma for sites i-CL and i-sGBL). For CL and sGBL, inset plot with expanded age axis shows older outliers. Dashed grey lines indicate *a priori* ^{14}C constraints on initial ice retreat.

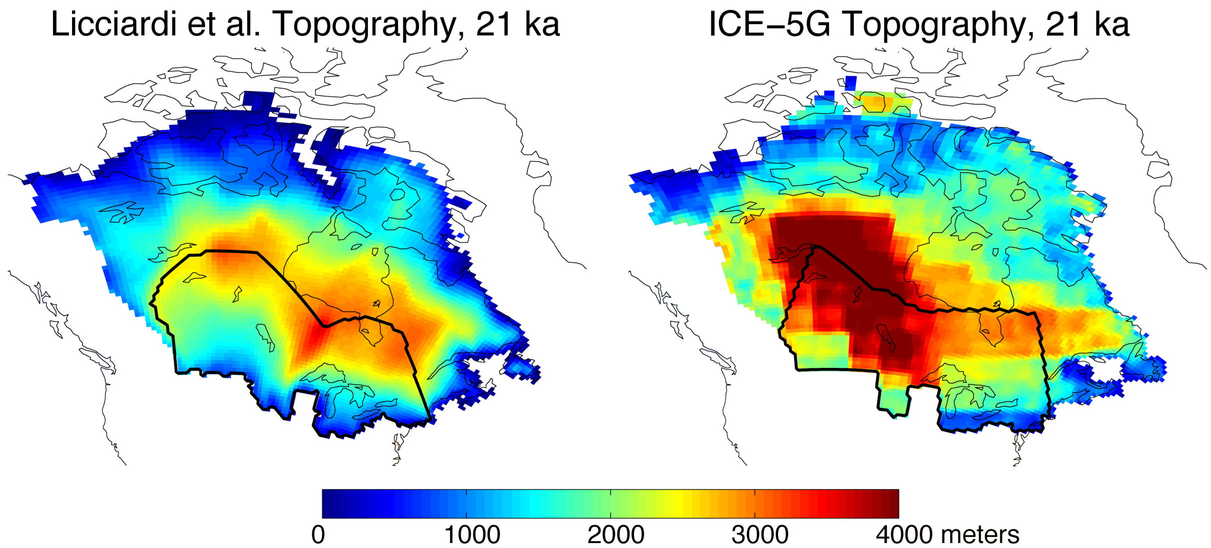

Fig. DR10. Comparison of the LIS topographies in the reconstruction used in our surface mass balance simulations (left; Licciardi et al., 1998) and the ICE-5G reconstruction (right; Peltier, 2004). Units are meters above 21 ka sea level. The region outlined in black indicates the area used to calculate the region-specific surface mass balance for the sLIS. This region is separated from the rest of the LIS using topographic ice drainage divides from the reconstruction. Because we focus only on the sLIS, we restrict our surface mass balance analysis to the two southernmost regions from the James Lobe to New England. Note: ICE-5G was not used in the analysis for this paper because it does not adequately resolve the low-elevation margins along the sLIS.

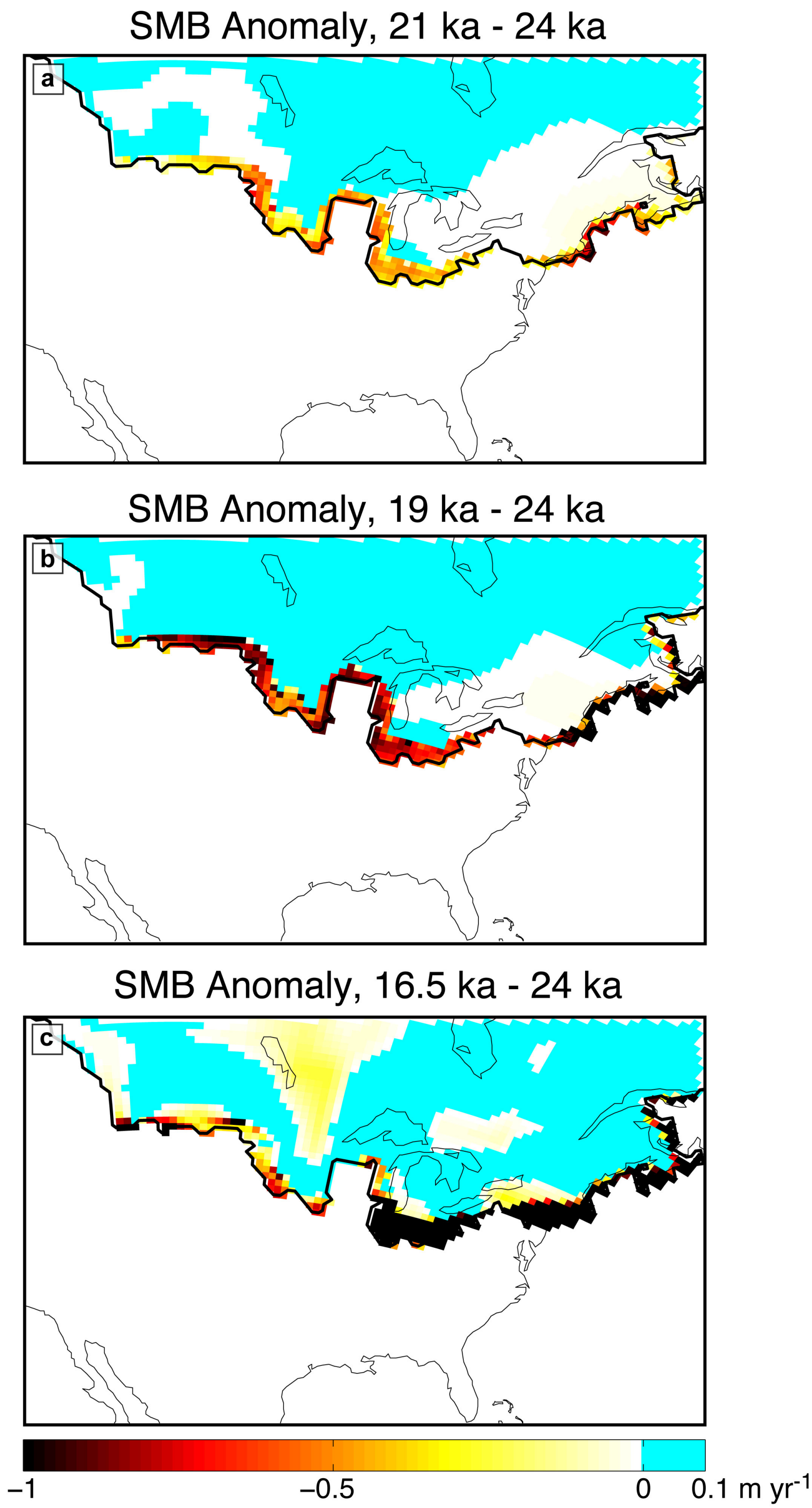

Fig. DR11. Modeled surface mass balance (SMB; units of meters water equivalent per year) anomalies relative to 24 ka at (**a**) 21 ka, (**b**) 19 ka, and (**c**) 16.5 ka.

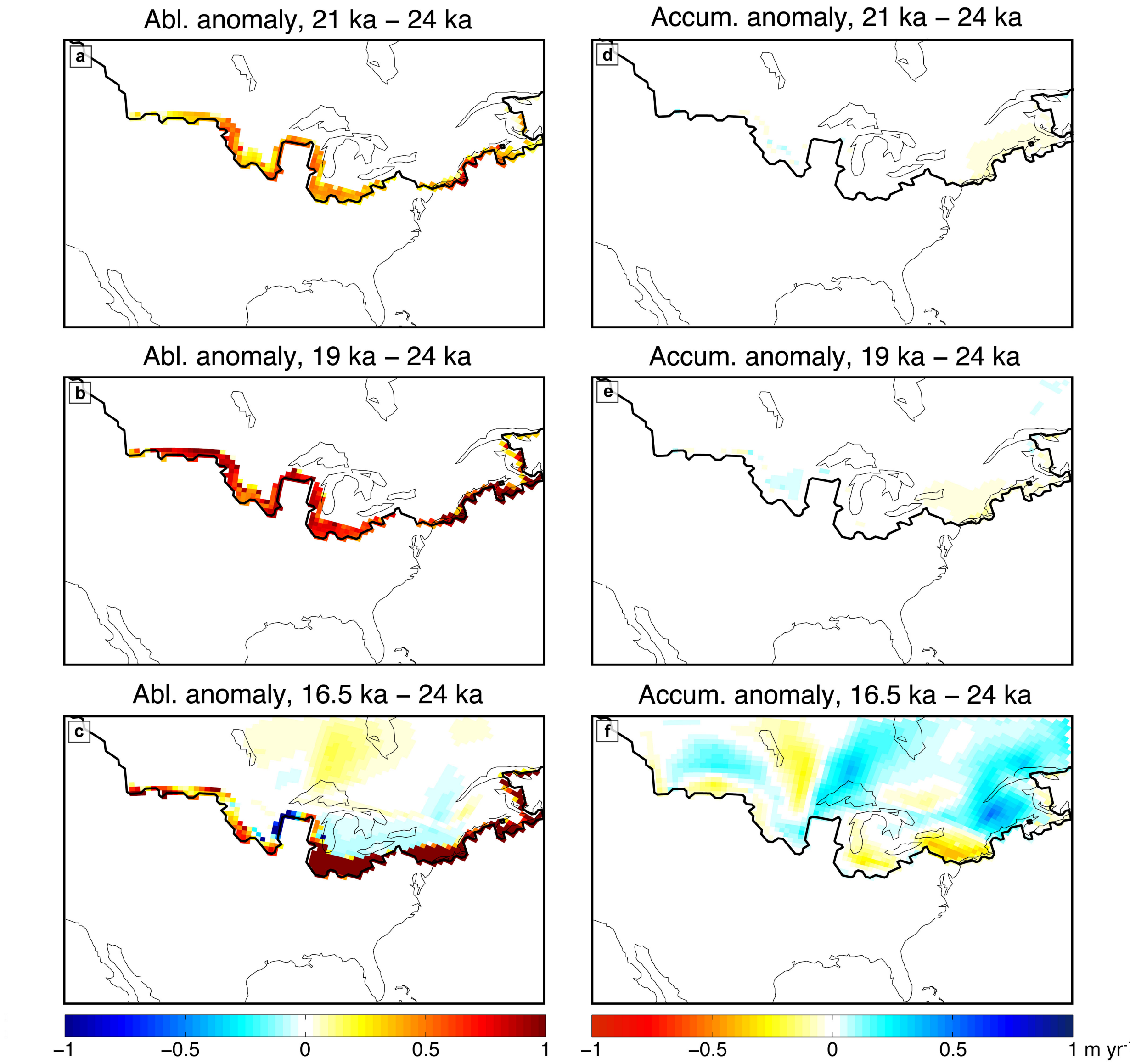

Fig. DR12. Ablation and accumulation anomalies for each of the SEBM simulations relative to 24 ka (units of meters water equivalent per year). (**a**) 21 ka ablation anomaly, (**b**) 19 ka ablation anomaly (**c**) 16.5 ka ablation anomaly, (**d**) 21 ka accumulation anomaly, (**e**) 19 ka accumulation anomaly (**f**) 16.5 ka accumulation anomaly.

Table DR1a. Cosmogenic sample information.

Sample	Latitude (DD)	Longitude (DD)	Modern Elevation (m asl)	Sample Lithology[a]	Thickness (cm)	Quartz (g)	Be Standard Used	AMS $^{10}Be/^{9}Be$ ratio (10^{-15})[b]	AMS Uncertainty (10^{-15})[c]	^{10}Be (atoms g^{-1})[d]	Uncertainty (atoms g^{-1})	^{10}Be age (ka)[e]
CL												
RCLC-09-02	45.469	-91.535	449	granite	3.0	41.626	Claritas	178.7	6.8	134339	5706	22.8 ± 1.0
RCLC-09-03	45.469	-91.534	449	granite	3.5	51.729	Claritas	200.1	6.0	120686	4087	20.6 ± 0.7
RCLC-09-04	45.470	-91.534	440	quartzite	2.0	45.557	Claritas	412.8	10.7	296900	8522	50.2 ± 1.5
RCLC-09-06	45.472	-91.531	461	granite	3.0	49.429	Claritas	236.3	9.2	152771	6527	25.6 ± 1.1
RCLC-09-13	45.480	-91.525	505	quartzite	2.0	48.448	Claritas	435.0	9.0	295706	7018	47.1 ± 1.2
RCLC-11-05	45.472	-91.534	444	granite	3.0	29.893	OSU Blue	255.0	11.0	141309	6309	24.1 ± 1.1
RCLC-11-06	45.471	-91.531	410	granite	2.5	29.922	OSU Blue	255.0	11.0	141035	6297	24.7 ± 1.1
RCLC-11-07	45.471	-91.532	432	granite	2.5	30.111	OSU Blue	326.0	11.0	179304	6352	30.7 ± 1.1
RCLC-11-08	45.472	-91.531	428	granite	3.0	22.242	OSU Blue	191.0	6.0	141880	4733	24.6 ± 0.8
RCLC-11-09	45.472	-91.530	439	granite	2.0	21.188	OSU Blue	491.0	11.0	385319	9495	65.6 ± 1.7
i-CL												
RCLC-11-01	45.504	-91.388	514	granite	3.0	29.421	OSU Blue	229.0	10.0	127824	5780	20.5 ± 0.9
RCLC-11-02	45.503	-91.388	482	granite	2.5	29.909	OSU Blue	214.0	7.0	118463	4094	19.5 ± 0.7
GM												
GOG-11-01	46.286	-90.794	507	granite	2.0	21.692	OSU Blue	119.0	5.0	90064	3964	14.4 ± 0.6
GOG-11-02	46.286	-90.794	538	granite	2.5	22.106	OSU Blue	103.0	5.0	76293	3864	11.9 ± 0.6
GOG-11-03	46.286	-90.794	538	granite	1.5	22.516	OSU Blue	107.0	4.0	77794	3078	12.1 ± 0.5
GOG-11-04	46.286	-90.794	531	granite	2.5	24.900	OSU Blue	128.0	6.0	84574	4124	13.3 ± 0.6
GOG-11-06	46.286	-90.794	518	granite	2.0	21.764	OSU Blue	144.0	26.0	108943	19976	17.2 ± 3.2
GOG-11-07	46.285	-90.795	522	granite	2.5	22.392	OSU Blue	123.0	6.0	90230	4574	14.3 ± 0.7
GOG-11-08	46.285	-90.795	524	granite	2.0	24.394	OSU Blue	135.0	7.0	91213	4894	14.4 ± 0.8
GOG-11-09	46.285	-90.795	527	granite	1.0	24.785	OSU Blue	117.0	6.0	77550	4128	12.1 ± 0.6
nGBL												
GBL-11-01	44.990	-89.316	447	granite	1.5	29.944	OSU Blue	356.0	14.0	196807	8033	33.1 ± 1.4
GBL-11-02	44.990	-89.316	445	granite	4.0	30.102	OSU Blue	245.0	8.0	134390	4631	23.2 ± 0.8
GBL-11-03	44.990	-89.317	436	granite	2.0	21.007	OSU Blue	226.0	6.0	178036	5103	30.3 ± 0.9
GBL-11-04	44.990	-89.316	438	granite	2.0	21.916	OSU Blue	162.0	6.0	121899	4741	20.9 ± 0.8
GBL-11-05	44.990	-89.316	438	granite	1.5	29.958	OSU Blue	271.0	12.0	149339	6832	25.4 ± 1.2
GBL-11-06	45.029	-89.269	465	granite	3.0	30.077	OSU Blue	260.0	9.0	143081	5198	24.0 ± 0.9
GBL-11-07	45.029	-89.269	465	granite	2.5	30.486	OSU Blue	262.0	8.0	141980	4600	23.8 ± 0.8
GBL-11-08	45.029	-89.269	465	granite	1.5	29.916	OSU Blue	215.0	9.0	118532	5152	19.7 ± 0.9
GBL-11-09	45.029	-89.269	465	granite	3.0	21.894	OSU Blue	213.0	7.0	160754	5580	27.0 ± 1.0
GBL-11-10	45.029	-89.269	465	granite	2.5	23.549	OSU Blue	198.0	8.0	138833	5842	23.3 ± 1.0

[a]All age calculations assume a density of 2.65 g cm^{-3} for granite and sandstone, 2.75 g cm^{-3} for quartzite.

[b]All AMS measurements are standardized to 07KNSTD.

[c]1-sigma AMS uncertanty

[d] ^{10}Be atom concentrations are blank-corrected (see text).

[e]All age calculations use standard atmosphere, modern elevation, and zero erosion. No shielding correction necessary.

^{10}Be ages are presented with 1-sigma analytical uncertainty.

Ages were calculated using the CRONUS Earth online calculator(v 2.2) with the NENA production rate and the Lal/Stone time-dependent scaling scheme (see text).

Table DR1b. Cosmogenic sample information (continued).

Sample	Latitude (DD)	Longitude (DD)	Modern Elevation (m asl)	Sample Lithology[a]	Thickness (cm)	Quartz (g)	Be Standard Used	AMS $^{10}Be/^{9}Be$ ratio (10^{-15})[b]	AMS Uncertainty (10^{-15})[c]	^{10}Be (atoms g^{-1})[d]	Uncertainty (atoms g^{-1})	^{10}Be age (ka)[e]
i-nGBL												
LCBC-11-01	45.227	-88.768	412	granite	2.0	35.844	Merck	124.9	7.0	102066	6019	17.9 ± 1.1
LCBC-11-02	45.227	-88.768	408	granite	2.0	38.394	Merck	128.5	10.4	109884	9181	19.3 ± 1.6
LCBC-11-03	45.227	-88.768	417	granite	1.5	38.471	Merck	134.0	5.6	114498	5020	19.9 ± 0.9
LCBC-11-04	45.227	-88.769	430	granite	2.0	38.069	Merck	110.2	5.4	95591	4981	16.5 ± 0.9
LCBC-11-05	45.227	-88.769	375	granite	2.0	39.342	Merck	78.4	3.7	65205	3306	11.8 ± 0.6
sGBL												
BH-09-01	43.398	-89.692	397	granite	2.0	40.278	Claritas	154.1	9.1	119507	7840	21.6 ± 1.4
BH-09-02	43.397	-89.692	419	quartzite	4.0	38.344	Merck	396.5	14.4	342928	13020	61.5 ± 2.4
BH-09-03	43.397	-89.692	411	sandstone	4.0	39.051	Merck	310.0	10.1	262284	9045	46.9 ± 1.7
BH-09-04	43.398	-89.693	427	granite	2.0	39.195	Merck	111.2	8.7	91498	7502	16.2 ± 1.3
BH-09-05	43.398	-89.693	431	granite	3.0	40.838	Claritas	153.9	9.3	117868	7871	20.9 ± 1.4
BH-09-06	43.398	-89.694	425	quartzite	3.0	40.023	Claritas	187.8	7.0	149105	6170	26.4 ± 1.1
BH-09-07	43.398	-89.695	425	sandstone	2.0	40.008	Claritas	190.5	8.2	151706	7226	26.7 ± 1.3
BH-09-08	43.399	-89.694	424	sandstone	4.0	44.319	Claritas	181.3	6.9	129017	5504	23.1 ± 1.0
BH-09-09	43.400	-89.692	404	quartzite	5.0	39.104	Merck	446.5	15.7	376692	13868	69.0 ± 2.7
BH-12-05	43.398	-89.686	363	granite	2.0	25.280	OSU Blue	113.0	13.0	73741	8670	13.8 ± 1.6
BH-12-06	43.397	-89.686	371	granite	2.3	24.862	OSU Blue	118.0	8.0	77596	5414	14.4 ± 1.0
BH-12-07	43.397	-89.686	364	granite	2.3	24.693	OSU Blue	133.0	8.0	89353	5535	16.7 ± 1.0
BH-12-09	43.397	-89.690	405	granite	2.0	25.269	OSU Blue	220.0	30.0	142500	19665	25.5 ± 3.6
i-sGBL												
BH-12-01	43.498	-89.637	366	granite	2.0	24.698	OSU Blue	158.0	7.0	104533	4814	19.4 ± 0.9
BH-12-02	43.501	-89.640	336	granite	1.3	24.337	OSU Blue	151.0	8.0	101423	5547	19.3 ± 1.1

[a]All age calculations assume a density of 2.65 g cm^{-3} for granite and sandstone, 2.75 g cm^{-3} for quartzite.

[b]All AMS measurements are standardized to 07KNSTD.

[c]1-sigma AMS uncertanty

[d] ^{10}Be atom concentrations are blank-corrected (see text).

[e]All age calculations use standard atmosphere, modern elevation, and zero erosion. No shielding correction necessary.

^{10}Be ages are presented with 1-sigma analytical uncertainty.

Ages were calculated using the CRONUS Earth online calculator(v 2.2) with the NENA production rate and the Lal/Stone time-dependent scaling scheme (see text).

Table DR2. Radiocarbon and calibrated ages used in construction of time-distance diagrams in Fig. 2 (main text).

	Sample ID	Radiocarbon Age (^{14}C years BP)	1 sigma error (^{14}C years)	Calibrated min* (cal. years BP)	Calibrated Max* (cal. years BP)	Median Calendar Age (cal. years BP)	1 sigma error (cal. years)	Reference
Green Bay Lobe	WIS-2022	26060	800	29443	30943	30193	750	Black, 1976
	CAM-252810	14500	70	17560	17789	17675	115	Maher et al., 1998
	CAM-291200	14210	90	17163	17446	17305	142	Maher et al., 1998
	CAM-291210	13980	190	16646	17248	16947	301	Maher et al., 1998
	CAM-291190	13150	120	15601	15994	15798	197	Maher et al., 1998
	WIS-2293	12965	200	15210	15802	15506	296	Maher and Mickelson, 1996
	Beta-119360	13370	90	15954	16224	16089	135	Mickelson et al., 2007
	WIS-431	13120	130	15530	15966	15748	218	Black, 1976
	W-1004	12880	130	15192	15598	15395	203	Maher and Mickelson, 1996
	W-1075	12520	160	14408	15081	14745	337	Maher and Mickelson, 1996
	W-1073	12260	120	13989	14496	14243	254	Maher and Mickelson, 1996
	2creeks_avg	11850	200	13465	13930	13698	233	Maher and Mickelson, 1996
	socha_2creeks	11690	70	13446	13572	13509	63	Socha, 2007
	socha_2creeks	12110	70	13847	14066	13957	110	Socha, 2007
	socha_2creeks	11210	100	12976	13198	13087	111	Socha, 2007
	socha_2creeks	11820	100	13552	13751	13652	100	Socha, 2007
	B4003	11620	50	13395	13538	13467	72	Kaiser, 1994
	b4005	11640	30	13430	13537	13484	54	Kaiser, 1994
	b4742	11560	40	13351	13445	13398	47	Kaiser, 1994
	eth8270	11865	65	13601	13744	13673	72	Kaiser, 1994
	eth8271	11760	90	13482	13708	13595	113	Kaiser, 1994
	eth8272	11915	100	13576	13842	13709	133	Kaiser, 1994
	eth8273	12035	60	13784	13959	13872	88	Kaiser, 1994
	eth8274	11885	100	13566	13795	13681	115	Kaiser, 1994
	eth8608	11965	95	13715	13980	13848	133	Kaiser, 1994
	eth8609	11890	95	13570	13792	13681	111	Kaiser, 1994
	eth8610	11805	95	13549	13742	13646	97	Kaiser, 1994
	eth8611	11980	95	13731	13980	13856	125	Kaiser, 1994
	eth8612	12015	90	13760	13981	13871	111	Kaiser, 1994
	wis1653	11690	130	13401	13708	13555	154	Kaiser, 1994
	DAL-340	9545	225	10584	11179	10882	298	Hughes and Merry, 1978
	W-3904	9780	250	10753	11607	11180	427	Hughes and Merry, 1978
	W-3866	9850	300	10784	11807	11296	512	Hughes and Merry, 1978
	DAL-338	10220	215	11419	12384	11902	483	Hughes and Merry, 1978
	W-3896	10330	300	11629	12565	12097	468	Hughes and Merry, 1978
	A-7878	9895	55	11232	11349	11291	59	Lowell et al., 1999b
	A-7876	9910	55	11240	11390	11315	75	Lowell et al., 1999b
	A-7877	9965	55	11267	11599	11433	166	Lowell et al., 1999b
	A-7879	10040	55	11399	11701	11550	151	Lowell et al., 1999b
	A-7881	10040	65	11396	11707	11552	156	Lowell et al., 1999b
	A-7883	10050	55	11404	11706	11555	151	Lowell et al., 1999b
	A-7880	10075	95	11397	11814	11606	209	Lowell et al., 1999b
	A-7882	10155	65	11650	11982	11816	166	Lowell et al., 1999b
	A-7875	10200	55	11774	12013	11894	120	Lowell et al., 1999b
	WIS-442	15560	150	18659	18957	18808	149	Bender et al., 1971
	WIS-1519	15940	150	19033	19426	19230	197	Steventon and Kutzbach, 1985
	WIS-1515	16580	120	19833	20171	20002	169	Steventon and Kutzbach, 1985
	MAR-1-P	17020	70	20427	20638	20533	106	Carson et al., 2012
	L-1064	13300	300	15514	16413	15964	450	Farrand et al., 1969
Northern Green Bay Lobe	CAM-252810	14500	70	17560	17789	17675	115	Maher et al., 1998
	CAM-291200	14210	90	17163	17446	17305	142	Maher et al., 1998
	CAM-291210	13980	190	16646	17248	16947	301	Maher et al., 1998
	CAM-291190	13150	120	15601	15994	15798	197	Maher et al., 1998
	WIS-2293	12965	200	15210	15802	15506	296	Maher and Mickelson, 1996
	L-1064	13300	300	15514	16413	15964	450	Farrand et al., 1969
Lake Michigan Lobe	ISGS-3021	23230	550	26885	27926	27406	521	Hansel and Johnson, 1996
	ISGS-1486	21460	470	25212	26201	25707	495	Garry et al., 1990
	ISGS-2484	21370	240	25470	25910	25690	220	Hansel and Johnson, 1996
	W-349	20340	500	23932	25148	24540	608	Hansel and Johnson, 1996
	ISGS-2047	20020	230	23809	24356	24083	274	Hansel and Johnson, 1996
	ISGS-3100	19830	190	23631	24088	23860	229	Hansel and Johnson, 1996
	ISGS-532	19680	460	23107	24207	23657	550	Hansel and Johnson, 1996
	UCIAMS-23773	15150	45	18342	18491	18417	75	Curry, 2008
	UCIAMS-23772	15740	150	18829	19171	19000	171	Curry, 2008
	UCIAMS-23765	17290	140	20651	21037	20844	193	Curry, 2008
	UCIAMS-23768	15125	45	18314	18466	18390	76	Curry, 2008
	UCIAMS-23770	17090	190	20371	20866	20619	248	Curry, 2008
	UCIAMS-23769	17250	60	20690	20900	20795	105	Curry, 2008
	OxA-W917-11	16700	90	20018	20280	20149	131	Curry, 2008

	OxA-W917-9	17610	270	20927	21654	21291	364	Curry, 2008
	ISGS-767	17690	270	21041	21764	21403	362	Hansel and Johnson, 1992
	UCIAMS-26260	17760	60	21385	21629	21507	122	Curry and Petras, 2011
	UCIAMS-26261	18210	60	21945	22188	22067	122	Curry and Petras, 2011
	OxA-W814-13	17540	130	20991	21391	21191	200	Curry et al., 1999
	ISGS-A-0164	16540	120	19779	20115	19947	168	Patterson et al., 2003
	ISGS-465	15240	120	18367	18642	18505	138	Hansel and Johnson, 1992
	ISGS-A-0165	14860	110	17938	18221	18080	142	Patterson et al., 2003
	ISGS-A-0143	14610	110	17648	17924	17786	138	Curry and Petras, 2011
	ISGS-1550	14330	200	17160	17705	17433	273	Hansel and Johnson, 1992
	UCIAMS-46831	14780	50	17895	18060	17978	83	Curry, 2008
	UCIAMS-26265	14860	40	17974	18142	18058	84	Curry and Petras, 2011
	ISGS-1570	14100	640	16234	17917	17076	842	Hansel and Johnson, 1996
	ISGS-1649	13890	120	16623	17031	16827	204	Hansel and Johnson, 1996
	UCIAMS-26262	14070	40	17009	17197	17103	94	Curry, 2008
	UCIAMS-26263	14110	35	17063	17256	17160	97	Curry, 2008
	UCIAMS-26264	14420	40	17490	17649	17570	80	Curry, 2008
	ISGS-1549	13870	170	16525	17064	16795	270	Hansel and Johnson, 1996
	UICAMS-46829	13650	40	16336	16547	16442	106	Curry, 2008
	UCIAMS-63075	13695	45	16387	16626	16507	120	Curry and Petras, 2011
	UCIAMS-63076	13910	35	16767	16984	16876	109	Curry and Petras, 2011
	ISGS-1378	13470	130	16019	16404	16212	193	Monaghan and Hansel, 1990
	L-1064	13300	300	15514	16413	15964	450	Farrand et al., 1969
	IGS-482	12410	120	14204	14764	14484	280	Hansel and Johnson, 1996
	ISGS-1061	11700	110	13423	13706	13565	142	Liu et al., 1986
	ISGS-1234	11650	170	13301	13704	13503	202	Garry et al., 1990
Miami/Scioto Lobes	22 (Beta-72287)	18460	90	22251	22456	22354	103	Glover et al., 2011
	DIC-243	14810	170	17831	18253	18042	211	Glover et al., 2011
	DIC-510	14890	130	17956	18275	18116	160	Glover et al., 2011
	CAMS-2409	11680	90	13408	13589	13499	91	Glover et al., 2011
	ISGS-1677	12210	150	13816	14392	14104	288	Glover et al., 2011
	ISGS-1055	13510	160	16041	16514	16278	237	Glover et al., 2011
	ETH-30202	15710	90	18842	19052	18947	105	Glover et al., 2011
	Beta-158291	11860	270	13420	14051	13736	316	Glover et al., 2011
	AA-45069	15810	140	18897	19236	19067	170	Glover et al., 2011
	AA-45069b	15350	100	18519	18736	18628	109	Glover et al., 2011
	AA-45073	15503	91	18674	18856	18765	91	Glover et al., 2011
	AA-45074	14986	98	18076	18344	18210	134	Glover et al., 2011
	AA-45077	14360	120	17317	17668	17493	176	Glover et al., 2011
	AA53435	15564	88	18733	18902	18818	85	Glover et al., 2011
	AA-45078	14600	91	17657	17900	17779	122	Glover et al., 2011
	AA-45079	16170	97	19366	19649	19508	142	Glover et al., 2011
	AA53419	15869	91	18987	19248	19118	131	Glover et al., 2011
	AA53425	16400	170	19585	19996	19791	206	Glover et al., 2011
	AA53442	16010	100	19184	19475	19330	146	Glover et al., 2011
	AA53429	10676	58	12596	12692	12644	48	Glover et al., 2011
	AA53418	15640	97	18780	18978	18879	99	Glover et al., 2011
	AA53423	16128	90	19326	19586	19456	130	Glover et al., 2011
	Beta-190863	16050	90	19240	19500	19370	130	Glover et al., 2011
	ETH-28523	15560	100	18718	18909	18814	96	Glover et al., 2011
	CAMS-27129	15630	150	18722	19037	18880	158	Glover et al., 2011
	CAMS-27130	15770	80	18910	19116	19013	103	Glover et al., 2011
	ETH-32177	14780	100	17854	18118	17986	132	Glover et al., 2011
	Beta-194054	13690	50	16376	16621	16499	123	Glover et al., 2011
	Beta-190864	13880	70	16675	16965	16820	145	Glover et al., 2011
	PITT-0227	19960	170	23809	24229	24019	210	Lowell et al., 1990
	PITT-0506	19310	170	23031	23478	23255	224	Lowell et al., 1990
	PITT-0507	20200	140	24093	24440	24267	174	Lowell et al., 1990
	PITT-0508	19200	140	22941	23344	23143	202	Lowell et al., 1990
	PITT-0509	19690	150	23531	23912	23722	191	Lowell et al., 1990
	OWU-76	17290	436	20338	21459	20899	561	Dyke, 2004
	OWU-83	14780	192	17753	18231	17992	239	Dyke, 2004

*Calibrated using Calib 7.0 and IntCal13 (Stuiver and Reimer, 1993; Reimer et al., 2013)

Supplementary References

Abe-Ouchi, A., Segawa, T., and Saito, F., 2007, Climatic conditions for modeling the Northern Hemisphere ice sheets throughout the ice age cycle: Climate of the Past, v. 3, p. 423-438.

Anslow, F.S., Hostetler, S., Bidlake, W.R., and Clark, P.U., 2008, Distributed energy balance modeling of South Cascade Glacier, Washington and assessment of model uncertainty: Journal of Geophysical Research, v. 113, F02019.

Argus, D.F. and Peltier, W.R., 2010, Constraining models of postglacial rebound using space geodesy: a detailed assessment of model ICE-5G (VM2) and its relatives: Geophysical Journal International, v. 181, p. 697-723.

Attig, J.W., Clayton, L., and Mickelson, D.M., 1985, Correlation of late Wisconsin glacial phases in the western Great Lakes area: Geological Society of America Bulletin, v. 96, p. 1585-1593.

Balco, G., Stone, J.O., Lifton, N.A., and Dunai, T.J., 2008, A complete and easily accessible means of calculating surface exposure ages or erosion rates from ^{10}Be and ^{26}Al measurements: Quaternary Geochronology, v. 3, p. 174-195.

Balco, G., Briner, J., Finkel, R.C., Rayburn, J.A., Ridge, J.C., and Schaefer, J.M., 2009, Regional beryllium-10 production rate calibration for late-glacial northeastern North America: Quaternary Geochronology, v. 4, p. 93-107.

Bender, M.M., Bryson, R.A., and Baerreis, D.A., 1971, University of Wisconsin radiocarbon dates IX: Radiocarbon, v. 13, p. 475-486.

Berger, A. and Loutre, M.F., 1991, Insolation values for the climate of the last 10 million years: Quaternary Science Reviews, v. 10, p. 297-317.

Bevington, P. and Robinson, D.K., 2002, Data reduction and error analysis for the physical sciences, 3rd Ed.: McGraw-Hill, Boston, 336 p.

Black, R.F., 1976, Quaternary geology of Wisconsin and upper Michigan, *in* Mahaney, W.C., ed., Quaternary Stratigraphy of North America: Stroudsber, PA, Dowden, Hutchinson, and Ross, p. 93-117.

Cannon, W.F., LaBerge, G.L., Klasner, J.S., Schulz, K.J., 2007, The Gogebic Iron Range--A sample of the northern margin of the Penokean fold and thrust belt: USGS Professional Paper 1730, 44 p.

Carlson, A.E., Anslow, F.S., Obbink, E.A., LeGrande, A.N., Ullman, D.J., and Licciardi, J.M., 2009, Surface-melt driven Laurentide Ice sheet retreat during the early Holocene: Geophysical Research Letters, v. 36, L24502.

Carlson, A.E., Ullman, D.J., Anslow, F.S., He, F., Clark, P.U., Liu, Z., and Otto-Bliesner, B.L., 2012, Modeling the surface mass-balance response of the Laurentide Ice Sheet to Bølling warming and its contribution to Meltwater Pulse 1A: Earth and Planetary Science Letters, v. 315-316, p. 24-29.

Carson, E.C., Hanson, P.R., Attig, J.W., and Young, A.R., 2012, Numeric control on the late-glacial chronology of the southern Laurentide Sheet derived from ice-proximal lacustrine deposits: Quaternary Research, v. 78, p. 583-589.

Clark, P.U., 1992, Surface form of the southern Laurentide Ice Sheet and implications to ice-sheet dynamics: Geological Society of America Bulletin, v. 104, p. 595-605.

Clark, P.U., Licciardi, J.M., MacAyeal, D.R., and Jenson, J.W., 1996, Numerical reconstruction of a soft-bedded Laurentide Ice Sheet during the last glacial maximum: Geology, v. 24, p. 679-682.

Clark, P.U., Dyke, A.S., Shakun, J.D., Carlson, A.E., Clark, J., Wohlfarth, B., Mitrovica, J.X., Hostetler, S.W., and McCabe, A.M., 2009, The Last Glacial Maximum: Science, v. 325, p. 710–714.

Clayton, L. and Attig, J.W., 1990, Geology of Sauk County, Wisconsin: Wisconsin Geological and Natural History Survey Information Circular, v. 67, 68 p.

Colgan, P.M., Bierman, P.R., Mickelson, D.M., and Caffee, M., 2002, Variation in glacial erosion near the southern margin of the Laurentide Ice Sheet, south-central Wisconsin, USA: Implications for cosmogenic dating of glacial terrains: Geological Society America Bulletin, v. 114, p. 1581-1591.

Corbett, L.B., Bierman, P.R., Graly, J.A., Neumann, T.A., and Rood, D.H., 2013, Constraining landscape history and glacial erosivity using paired cosmogenic nuclides in Upernavik, northwest Greenland: Geological Society of America Bulletin, doi:10.1130/B30813.1.

Curry, B.B., Grimley, D.A., and Stravers, J.A., 1999, Quaternary geology, geomorphology, and climatic history of Kane County, Illinois: Illinois State Geological Survey Guidebook, v. 28, 40 p.

Curry, B.B., 2008, Deglacial History and Paleoenvironments of North-eastern Illinois, 54th Midwest Friends of the Pleistocene Field Conference, May 16-18, 2008: Illinois State Geological Survey Open File Series 2008-1, 175 p.

Curry, B. and Petras, J., 2011, Chronological framework for the deglaciation of the Lake Michigan lobe of the Laurentide Ice Sheet from ice-walled lake deposits: Journal of Quaternary Science, v. 26, p. 402-410.

Desilets, D., Zreda, M. and Prabu, T., 2006, Extended scaling factors for in situ cosmogenic nuclides: new measurements at low latitude: Earth and Planetary Science Letters, v. 246, p. 265-276.

Dunai, T., 2001, Influence of secular variation of the magnetic field on production rates of in situ produced cosmogenic nuclides: Earth and Planetary Science Letters, v. 193, p. 197-212.

Duynkerke, P.D. and van den Broeke, M.R., 1994, Surface energy balance and katabatic flow over glacier and tundra during GIMEX-91: Global and Planetary Change, v. 9, p. 17-28.

Dyke, A.S., 2004, An outline of North American deglaciation with emphasis on central and northern Canada, *in* Ehlers, J. and Gibbard, P.L., eds., Quaternary Glaciations-Extent and Chronology, Part II: Amsterdam, Elsevier Science and Technology Books, p. 373-424.

Dyke, A.S., Andrews, J.T., Clark, P.U., England, J.H., Miller, G.H., Shaw, J., and Veillette, J.J., 2002, The Laurentide and Innuitian ice sheets during the Last Glacial Maximum: Quaternary Science Reviews, v. 21, p. 9-31.

Eckberg, M.P., Lowell, T.V., and Stuckenrath, R., 1993, Late Wisconsin glacial advance and retreat patterns in southwestern Ohio, USA: Boreas v. 22, p. 189-204.

Farrand, W.R., Benninghoff, W.S., Zhner, R., 1969, Cary-Port Huron Interstade: evidence from a buried bryophyte bed, Cheboygan County, Michigan: Geological Society of America Special Paper, v. 123, p. 249-262.

Garry, C.E., Baker, R.W., Schwert, D.P., and Schneider, A.F., 1990, Environmental analysis of a Twocreekan-aged beetle (Coleoptera) assemblage from Kewaunee, Wisconsin: Geological Society of America Special Paper, v. 251, p. 57-66.

Glover, K.C., Lowell, T.V., Wiles, G.C., Pair, D., Applegate, P., and Hajdas, I., 2011, Deglaciation, basin formation and post-glacial climate change from a regional network of sediment core sites in Ohio and eastern Indiana: Quaternary Research, v. 76, p. 401-410.

Grainger, M.E. and Lister, H., 1966, Wind speed, stability and eddy viscosity over melting ice surfaces: Journal of Glaciology, v. 6, p. 101-127.

Greuell, W. and Konzelmann, T., 1994, Numerical modelling of the energy balance and the englacial temperature of the Greenland Ice Sheet. Calculations for the ETH-Camp location (West Greenland, 1155 m a.s.l.): Global and Planetary Change, v. 9, p. 91-114.

Hansel, A.K. and Johnson, W.H., 1992, Fluctuations of the Lake Michigan lobe during the late Wisconsin subepisode: Sveriges Geologiska Undersökning, v. 81, p. 133-144.

Hansel, A.K. and Johnson, W.H., 1996, Wedron and Mason Groups: Lithostratigraphic reclassification of deposits of the Wisconsin Episode, Lake Michigan Lobe area: Illinois State Geological Survey Bulletin, v. 104, 116 p.

Hooyer, T.S., 2007, Evolution of glacial Lake Oshkosh and the Fox River Lowland, *in* Hooyer, T.S., ed., Late-glacial history of east-central Wisconsin, Guide Book for the 53rd Midwest Friends of the Pleistocene Field Conference, May 18-20, 2007, Oshkosh, WI: Wisconsin Geological and Natural History Survey Open-File Report 2007-01, p. 1-16.

Hughes, L. and Merry, W.J., 1978, Marquette buried forest 9,850 years old: American Association for the Advancement of Science, Abstract for Annual Meeting, no. 12-14.

Johnson, M.D., 1986, Pleistocene geology of Barron County, Wisconsin: Wisconsin Geological and Natural History Survey Information Circular, v. 55, 42 p.

Kaiser, K.F., 1994, Two Creeks Interstade dated through dendrochronology and AMS: Quaternary Research, v. 42, p. 288-298.

Lal, D., 1991, Cosmic ray labeling of erosion surfaces: in situ nuclide production rates and erosion models: Earth and Planetary Science Letters, v. 104, p. 424-439.

Lambeck, K., Purcell, A., Zhao, J., and Svensson, N.O., 2010, The Scandinavian Ice Sheet: from MIS 4 to the end of the Last Glacial Maximum: Boreas, v. 39, p. 410-435.

Licciardi, J.M., Clark, P.U., Jenson, J.W., and Macayeal, D.R., 1998, Deglaciation of a soft-bedded Laurentide Ice Sheet: Quaternary Science Reviews, v. 17, p. 427-448.

Lifton, N.A., Bieber, J.W., Clem, J.M., Duldig, M.L., Evenson, P., Humble, J.E., and Pyle, R., 2005, Addressing solar modulation and long-term uncertainties in scaling secondary cosmic rays for in situ cosmogenic nuclide applications: Earth and Planetary Science Letters, v. 239, p. 140-161.

Lowell, T.V., Savage, K.M., Brockman, C.S., and Stuckenrath, R., 1990, Radiocarbon analyses from Cincinnati, Ohio, and their implications for glacial stratigraphic interpretations: Quaternary Research, v. 34, p. 1-11.

Lowell, T.V., Larson, G.J., Hughes, J.D., and Denton, G.H., 1999a, Age verification of the Lake Gribben forest bed and the Younger Dryas advance of the Laurentide Ice Sheet: Canadian Journal of Earth Sciences, v. 36, p. 383-393.

Lowell, T.V., Hayward, R.K. and Denton, G.H., 1999b, Role of climate oscillations in determining ice-margin position: hypothesis, examples, and implications: Geological Society of America Special Paper, v. 337, p. 193- 203.

Maher, L.J., Jr. and Mickelson, D.M., 1996, Palynological and radiocarbon evidence for deglaciation events in the Green Bay Lobe, Wisconsin: Quaternary Research, v. 46, p. 251-259.

Maher, L.J., Jr., Miller, N.G., Baker, R.G., Curry, B.B., and Mickelson, D.M., 1998, Paleobiology of the sand beneath the Valders diamicton at Valders, Wisconsin: Quaternary Research, v. 49, p. 208-221.

Mickelson, D.M., 1986, Glacial and related deposits of Langlade County, Wisconsin: Wisconsin Geological and Natural History Survey Information Circular, v. 52, 30 p.

Mickelson, D.M., Hooyer, T.S., Socha, B.J. and Winguth, C., 2007, Late glacial ice advances and vegetation changes in east-central Wisconsin, *in* Hooyer, T.S., ed., Late-glacial history of east-central Wisconsin, Guide Book for the 53rd Midwest Friends of the Pleistocene Field Conference, May 18-20, 2007, Oshkosh, WI: Wisconsin Geological and Natural History Survey Open-File Report 2007-01, p. 73-87.

Monaghan, G.W. and Hansel, A.K., 1990, Evidence for the intra-Glenwood (Mackinaw) low-water phase of glacial Lake Chicago: Canadian Journal of Earth Science, v. 27, p. 1236-1241.

Mudrey, M.G., Brown, B.A., and Greenberg, J.K., 1982, Bedrock geologic map of Wisconsin: University of Wisconsin-Extension, Geological and Natural History Survey.

Murray, D.S., Carlson, A.E., Singer, B.S., Anslow, F.S., He, F., Caffee, M., Marcott, S.A., Liu Z. and Otto-Bliesner, B.L., 2012, Northern Hemisphere forcing of the last deglaciation in southern Patagonia: Geology, v. 40, p. 631-634.

Patterson, C.J., Hansel, A.K., Mickelson, D.M., Quade, D.J., Bettis III, E.A., Colgan, P.M., McKay, E.D., Stumpf, A.J., 2003, Contrasting glacial landscapes created by ice lobes of the southern Laurentide Ice Sheet, *in* Eastbrook, D.J., ed., Quaternary Geology of the United States, INQUA 2003 Field Guide Volume: Reno, Desert Research Institute, p. 135-154.

Peltier, W.R., 2004, Global glacial isostasy and the surface of the ice-age earth: the ICE-5G (VM2) model and GRACE: Annual Reviews of Earth and Planetary Science, v. 32, p. 111-149.

Reimer, P.J. and 29 others, 2013, IntCal13 and Marine13 radiocarbon age calibration curves 0-50,000 years cal BP: Radiocarbon, v. 55, p. 1869-1887.

Rinterknecht, V.R., Clark, P.U.,, Raisbeck, G.M., Yiou, F., Bitinas, A., Brook, E.J., Marks, L., Zelcs, V., Lunkka, J.-P., Pavlovskaya, I.E., Piotrowski, J.A., and Raukas, A., 2006, The last deglaciation of the southeastern sector of the Scandinavian Ice Sheet: Science, v. 311, p. 1449-1452.

Schmidt, G.A., and 43 others, 2014, Configuration and assessment of the GISS ModelE2 contributions to the CMIP5 archive: Journal of Advances in Modeling Earth Systems, in press.

Schulte, L.A., Mladenoff, D.J., Crow, T.R., Merrick, L.C., and Cleland, D.T., 2007, Homogenization of northern U.S. Great Lakes forests due to land use: Landscape Ecology, v. 22, p. 1089-1103.

Smeets, C.J.P.P. and van den Broeke, M.R., 2008, Temporal and spatial variations off the aerodynamic roughness length in the ablation zone of the Greenland ice sheet: Boundary-Layer Meteorology, v. 128, p. 315-338.

Socha, B.J., 2007, Evidence of tundra plants overridden by ice approximately 16,000 cal yr BP, Sherwood, Wisconsin, Calumet County, *in* Hooyer, T.S., ed., Late-glacial history of east-central Wisconsin, Guide Book for the 53rd Midwest Friends of the Pleistocene Field Conference, May 18-20, 2007, Oshkosh, WI: Wisconsin Geological and Natural History Survey Open-File Report 2007-01, p. 73-87.

Steventon, R.L. and Kutzbach, J.E., 1985, University of Wisconsin radiocarbon dates XXII: Radiocarbon, v. 27, p. 455-469.

Stone, J.O., 2000, Air pressure and cosmogenic isotope production: Journal of Geophysical Research, v. 105, p. 23753-23759.

Stuiver, M. and Reimer, P.J., 1993, Extended ^{14}C data base and revised CALIB 3.0 ^{14}C age calibration program: Radiocarbon, v. 35, p. 215-230.

Tarasov, L. and Peltier, W.R., 2004, A geophysically constrained large ensemble analysis of the deglacial history of the North American ice-sheet complex: Quaternary Science Reviews, v. 23, p. 359-388.

Tarasov, L., Dyke, A.S., Neal, R.M., Peltier, W.R., 2012, A data-calibrated distribution of deglacial chronologies for the North American ice complex from glaciological modeling: Earth and Planetary Science Letters, v. 315-316, p. 30-40.

Ullman, D.J., LeGrande, A.N., Carlson, A.E., Anslow, F.S., and Licciardi, J.M., 2014, Assessing the impact of Laurentide Ice-Sheet topography on glacial climate: Climate of the Past, v. 10, p. 487-507.

van de Berg, W.J., van den Broeke, M., Ettema, J., van Meijgaard, E., Kaspar, F., 2011, Significant contribution of insolation to Eemian melting of the Greenland ice sheet: Nature Geoscience, v. 4, p. 679-683.

van de Wal, R.S.W., 1996, Mass-balance modelling of the Greenland ice sheet: a comparison of an energy-balance and a degree-day model, Annals of Glaciology, v. 23, p. 36-45.